$\mathcal{PT}$ symmetry, induced mechanical lasing, and tunable force sensing in a coupled-mode optically levitated nanoparticle

Sandeep Sharma [1,2,*] A. Kani,[2] and M. Bhattacharya [2]

[1]*Department of Physics, Korea Advanced Institute of Science and Technology (KAIST), Daejeon 34141, South Korea*

[2]*School of Physics and Astronomy, Rochester Institute of Technology, 84 Lomb Memorial Drive, Rochester, New York 14623, USA*

(Received 8 July 2021; accepted 23 March 2022; published 8 April 2022)

We theoretically investigate $\mathcal{PT}$ symmetry, induced mechanical lasing, and force sensing in an optically levitated nanoparticle with coupled oscillation modes. The coupling in the levitated system is created by the modulation of an asymmetric optical potential in the plane transverse to the beam trapping the nanoparticle. We show that such a coupling can lead to $\mathcal{PT}$-symmetric mechanical behavior for experimentally realistic parameters. Further, by examining the phonon dynamics and the second-order coherence of the nanoparticle modes, we determine that induced mechanical lasing is also possible. Finally, we demonstrate that tunable ultrasensitive force sensing ($\sim zN/\sqrt{Hz}$) can be engineered in the system. Our studies represent an advance in the fields of coherent manipulation of coupled degrees of freedom of levitated mechanical oscillators and their application for sensing.

DOI: 10.1103/PhysRevA.105.043505

I. INTRODUCTION

Coupled optomechanical systems have garnered a lot of attention in recent years owing to their potential applications in the fields of sensing [1–4], quantum information processing [5–7], and entanglement [8,9]. In connection with these applications, a variety of phenomena such as $\mathcal{PT}$ (parity-time) symmetry [10,11], quantum synchronization [12,13], photon blockade [14], quantum state transfer [15,16], etc., have been studied in the coupled systems. Most of these proposals involved coupled cavities or coupled clamped nanomechanical resonators, which may be less efficient in obtaining high-fidelity entanglement, quantum state transfer, ultrasensitive sensing, etc., owing to their high decoherence rates [17].

In contrast, realizing a coupled optomechanical configuration using an optically levitated system can be advantageous in overcoming this difficulty as these well-isolated systems are known to have very low decoherence rates [18,19]. Indeed, because they present such advantages, optically levitated systems have been used in applications such as force sensing [20,21], magnetic sensing [22], and rotational sensing [23]. Apart from these uses, optically levitated systems have also been used to study squeezing [24], bistability [25], superposition states [26,27], phonon lasing [28], etc. However, all these studies are mainly focused on using a single mechanical mode of the optically levitated system.

Recently, coherent dynamics of a two-mode-coupled levitated system have been studied by Frimmer *et al.* [29]. In their work, they have coupled the two transverse modes of an optically levitated nanoparticle by modulating an asymmetric trap potential in the transverse plane of the system. By exploiting this coupling, they have implemented cooling of the transverse modes in this system. However, to the best of our knowledge, apart from the abovementioned studies on coherent dynamics, not much has been explored about this coupled nanoparticle system. Hence, it is timely and important to explore different quantum phenomena arising in this coupled-mode system. Specifically, realization of a few phenomena such as $\mathcal{PT}$ symmetry and simultaneous lasing and sensing in this system can be advantageous because these can be further used to study the resulting phenomena of $\mathcal{PT}$-symmetric phonon lasing [30], squeezing enhancement [31], generation of nonclassical state [32], efficient quantum state transfer [33], quantum synchronization [34], and ultrasensitive sensing [35], which has potential application towards imaging [36] and quantum information processing [37]. Also, due to low decoherence rates, levitated coupled-mode systems can show higher efficiency in realizing the above phenomena than the conventional optomechanical systems. Apart from this, study of this simple coupled-mode system can be a basis for future exploration of the aforementioned phenomena in more complicated systems such as two or more particle coupled levitated systems, wherein multimode coupling can arise [38].

Consequently, in this work we propose to use the coupled-mode levitated nanoparticle as a tool box for studying the aforementioned phenomena (see Fig. 1). The coupling is introduced by manipulating the trap potential in the plane transverse to the trapping beam, which propagates along the z axis, as proposed by Frimmer *et al.* [29]. The modulation of the asymmetric potential results in the coupling of the two transverse oscillation modes x and y. By suitably amplifying and cooling the mechanical motion in the two modes, respectively, we find that the system can be driven into the $\mathcal{PT}$-symmetric regime. Numerical studies of phonon dynamics and second-order coherence imply that the system remains in a thermal state in this regime. However, we show

*quanta.sandeep@gmail.com

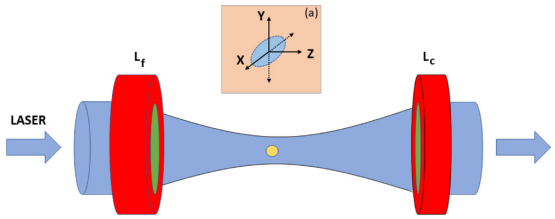

FIG. 1. A schematic diagram for the levitated nanoparticle system considered in this work. The lens L_f is used to trap the nanoparticle at the focus of the trap laser and the information about particle position is collected by the lens L_c to be processed. The inset shows an asymmetric potential created in the transverse x-y plane at the focus of the trap laser.

that when one of the modes is a lasing mode then the coupling drives the other modes also towards lasing. We also show that when a nonlinearly damped mode is coupled to a gain mode both the modes achieve lasing. Finally, we exploit the mode-mode coupling to achieve highly tunable ultrasensitive force sensing. We find that in the strong-coupling regime, weak forces can be measured with high sensitivity at different frequencies due to their tunability using this system.

In our simulations we use realistic experimental parameters and take into account relevant sources of noise and dissipation. Our work on analyzing various implications of modal coupling in an optically levitated nanoparticle opens up new possibilities for coherent manipulation and sensing using these highly isolated systems. In the remainder of this paper, we introduce our theoretical formulation in Sec. II, present the results and discussion in Sec. III, and present our conclusions in Sec. IV.

II. THEORETICAL FORMULATION

A. Model

We consider a single dielectric nanoparticle of mass m optically trapped in the potential created by a focused Gaussian beam under high vacuum, as shown in Fig. 1. The created optical potential is harmonic to a good approximation around the focus of the Gaussian beam. Hence, the trapped nanoparticle can be considered as a harmonic oscillator, whose three modes of oscillation are decoupled for small amplitudes, along the three principal axes x, y, and z, respectively [39].

In this paper, we concentrate on the particle dynamics in the x-y plane only, while freezing the particle motion along the z direction using feedback cooling. Further, the coupling of the motion along the x and y directions is achieved by modulating the polarization of the trap laser beam using an electro-optic modulator [29]. This modulation varies the asymmetric potential in the x-y plane, thereby coupling the modes. In order to study the dynamics of the coupled-mode system, we write the master equation for this system [28,40] as

$$\dot{\rho}_m = -i\sum_{j=x,y}\left\{\omega_j[a_j^\dagger a_j,\rho_m] + \left(\frac{\gamma_{gj}-\gamma_{aj}}{2}\right)[Q_j,\{P_j,\rho_m\}]\right\} - \sum_{j=x,y}\left(\frac{D_{tj}}{2}\mathcal{D}[Q_j]\rho_m - \frac{D_j}{2}\mathcal{D}[P_j]\rho_m\right) - \sum_{j=x,y}\left(i\gamma_{cj}[Q_j^3,\{P_j,\rho_m\}] - \Gamma_{cj}\mathcal{D}[Q_j^3]\rho_m\right) + i\frac{\kappa\delta}{m\sqrt{\omega_x\omega_y}}\cos(\omega_r t)[Q_xQ_y,\rho_m], \quad (1)$$

where ρ_m is the density matrix for the two-dimensional coupled system and the dimensionless position and momentum operators for the nanoparticle are denoted as Q_j and P_j, respectively. Here, $j \in \{x, y\}$ and symbolizes the two transverse modes x and y, respectively. Further, the commutators and anticommutators are represented by square [ ] and curly brackets { }, respectively. The mechanical modes are also represented by phonon creation ($a_j^\dagger$) and annihilation (a_j) operators that obey the bosonic commutation relation $[a, a^\dagger] = 1$. The Lindblad superoperator $\mathcal{D}[\mathcal{O}]$ is defined as

$$\mathcal{D}[\mathcal{O}] = \mathcal{O}^\dagger\mathcal{O}\rho + \rho\mathcal{O}^\dagger\mathcal{O} - 2\mathcal{O}^\dagger\rho\mathcal{O}. \quad (2)$$

The first term on the right-hand side of Eq. (1) corresponds to the harmonic motion of the system with frequencies ω_x and ω_y in the directions x and y, respectively. The second term represents damping (antidamping) due to the surrounding gas (linear feedback amplification) of the system with the rate γ_{gj} (γ_{aj}) [28]. However, in our case, linear amplification of only one of the modes is of interest, namely, the y mode of the coupled system. The third term depicts the net momentum diffusion with the rate D_{tj} ($= A_{tj} + D_{pj} + 2\Gamma_{aj}$), due to photon scattering (A_{tj}), gas scattering (D_{pj}), and linear feedback amplification back-action (Γ_{aj}). Further, the back-action rates Γ_{aj} are small in comparision to the rates A_{tj} and D_{pj} and, hence, can be neglected [28]. The fourth term represents the position diffusion (due to gas scattering) with the rate D_j. The fifth and sixth terms appear due to nonlinear feedback and its concomitant back-action effect, respectively. The rates of feedback cooling and cooling back-action are given by γ_{cj} and Γ_{cj}, respectively. The last term in Eq. (1) arises due to the coupling of the two transverse modes, x and y. The coupling is introduced by periodically rotating the asymmetric potential around the z axis by a small angle δ at the frequency ω_r ($\approx \omega_y - \omega_x$). Further, $\kappa \simeq m(\omega_y^2 - \omega_x^2)/2$ denotes the change in trap stiffness due to the asymmetry in the trapping potential. Throughout this paper, we analyze the effect of this coupling on the dynamics of the system and its relation to the realization of various interesting and useful phenomena.

B. Quantum Langevin equations

In order to study the effect of coupling on the position dynamics of both the modes of the coupled system, we use the full quantum Langevin equations of motion including all quantum fluctuations for the system, derived from Eq. (1). The complete equations of motion for the coupled system are given as

$$\dot{Q}_x = \omega_x P_x, \quad (3)$$

$$\dot{P}_x = -\omega_x Q_x - 2\left(\gamma_{gx} + 3\gamma_{cx}Q_x^2\right)P_x + \frac{\kappa\delta}{m\sqrt{\omega_x\omega_y}}\cos(\omega_r t)Q_y,$$

$$+\sqrt{\frac{2K_BT\gamma_{gx}}{\hbar\omega_x}}\xi_T+\sqrt{D_{tx}}\xi_{\mathrm{Fa}}+12Q_x^2\sqrt{\frac{\Gamma_{cx}^2}{\gamma_{cx}}}\xi_{\mathrm{Fc}}, \tag{4}$$

$$\dot{Q}_y=\omega_yP_y, \tag{5}$$

$$\dot{P}_y=-\omega_yQ_y-2\big(\gamma_{gy}-\gamma_{ay}+3\gamma_{cy}Q_y^2\big)P_y+\frac{\kappa\delta}{m\sqrt{\omega_x\omega_y}}\cos(\omega_rt)Q_x+\sqrt{\frac{2K_BT\gamma_{gy}}{\hbar\omega_y}}\xi_T+\sqrt{D_{ty}}\xi_{\mathrm{Fa}}+12Q_y^2\sqrt{\frac{\Gamma_{cy}^2}{\gamma_{cy}}}\xi_{\mathrm{Fc}}, \tag{6}$$

where the correlations corresponding to the zero-mean noise from the environment (ξ_T), the feedback amplification (ξ_{Fa}), and the cooling (ξ_{Fc}) are represented as $\langle\xi_T(t)\xi_T(t')\rangle=\delta(t-t')$, $\langle\xi_{\mathrm{Fa}}(t)\xi_{\mathrm{Fa}}(t')\rangle=\delta(t-t')$, and $\langle\xi_{\mathrm{Fc}}(t)\xi_{\mathrm{Fc}}(t')\rangle=\delta(t-t')$, respectively.

Now, in order to further simplify the above equations of motion, we use the following transformations:

$$Q_x=Q_0\mathrm{Re}\left\{a_x(t)\ \exp\left[i\left(\omega_0-\frac{\omega_r}{2}\right)t\right]\right\}, \tag{7}$$

$$Q_y=Q_0\mathrm{Re}\left\{a_y(t)\ \exp\left[i\left(\omega_0+\frac{\omega_r}{2}\right)t\right]\right\}, \tag{8}$$

where Q_0 is the initial amplitude of the oscillation modes, $\omega_0=\sqrt{\omega_x^2+\omega_y^2}/2$ is the carrier frequency, and the complex amplitudes for the oscillation modes along the x mode and the y mode are represented as a_x and a_y, respectively.

In our present work we are interested in studying the dynamics of the mean position for both the modes in the classical limit [41]. Hence, we neglect the quantum fluctuations and use the slowly varying amplitude approximation and the rotating-wave approximation to obtain the mean-value equations for the oscillation amplitudes of the coupled system as

$$\langle\dot{a}_x\rangle=-\frac{i}{2}(\Delta-i\Gamma_x)\langle a_x\rangle+i\beta_x\langle a_y\rangle, \tag{9}$$

$$\langle\dot{a}_y\rangle=i\beta_y\langle a_x\rangle+\frac{i}{2}(\Delta+i\Gamma_y)\langle a_y\rangle, \tag{10}$$

where $\Delta=\omega_1-\omega_r$, $\omega_1=(\omega_y^2-\omega_x^2)/2\omega_0$, $\Gamma_x=2(\gamma_{gx}+6\gamma_{cx}\langle a_x\rangle^2)$, $\Gamma_y=2(\gamma_{gy}-\gamma_{ay}+6\gamma_{cy}\langle a_y\rangle^2)$, $\beta_x=\omega_3\sqrt{\omega_x/\omega_y}$, $\beta_y=\omega_3\sqrt{\omega_y/\omega_x}$, and $\omega_3=[\delta(\omega_y^2-\omega_x^2)]/2\omega_0$. A detailed description of the analysis for deriving the above equation of motion is provided in the Appendix. Further, we can study the dynamics of phonon population in both modes via $|a_x(t)|^2$ and $|a_y(t)|^2$. In the classical limit, $|a_x(t)|^2$ and $|a_y(t)|^2$ give the description of phonon dynamics of the system. The study of phonon dynamics is very important as a saturationlike behavior of the phonon number can indicate lasing action in the system [28]. However, such behavior in the phonon dynamics is necessary but not sufficient for validating lasing action. Therefore, we also study the second-order coherence for the coupled-mode system in the following section.

C. Second-order coherence

Study of the second-order coherence is useful in characterizing various quantum states of a system. For example, a system in a thermal state has a Lorentzian $g^{(2)}(\tau)$ with $1\leqslant g^{(2)}(\tau)\leqslant 2$, and that in a coherent state has a constant $g^{(2)}(\tau)=1$ indicating the presence of lasing [42]. Finally, $0\leqslant g^{(2)}(\tau)<1$ represents a system in a nonclassical state [43]. Hence, to characterize the coupled-mode levitated system, we also study the second-order correlation function for it. The second-order correlation function can be expressed in terms of the creation and annihilation operators as

$$g_j^{(2)}(\tau)=\frac{\langle\hat{a}_j^\dagger(t)\hat{a}_j^\dagger(t+\tau)\hat{a}_j(t+\tau)\hat{a}_j(t)\rangle}{\langle\hat{a}_j^\dagger(t)\hat{a}_j(t)\rangle^2}, \tag{11}$$

where $\hat{a}_j^\dagger=(Q_j-iP_j)/2$ and $\hat{a}_j=(Q_j+iP_j)$, with $j\in\{x,y\}$. Further, $\langle\ \rangle$ indicates an ensemble average and τ represents the time delay.

III. RESULTS AND DISCUSSION

A. $\mathcal{PT}$ symmetry

In this subsection, we theoretically realize $\mathcal{PT}$ symmetry in a coupled-mode levitated nanoparticle. With this aim in mind, we first rewrite the dynamical equations Eqs. (9) and (10) into the following matrix form:

$$i\begin{bmatrix}\langle\dot{a}_x\rangle\\ \langle\dot{a}_y\rangle\end{bmatrix}=H\begin{bmatrix}\langle a_x\rangle\\ \langle a_y\rangle\end{bmatrix}, \tag{12}$$

where H is the non-Hermitian Hamiltonian for the coupled-mode system and is described as

$$H=\begin{bmatrix}\frac{1}{2}(\Delta-i\Gamma_x) & -\beta_x\\ -\beta_y & -\frac{1}{2}(\Delta+i\Gamma_y)\end{bmatrix}. \tag{13}$$

Next, we study the behavior of the eigenvalues of the Hamiltonian H, which are given by

$$\lambda_\pm=\frac{-(C_2-C_1)\pm\sqrt{(C_2-C_1)^2+4(\beta^2+C_1C_2)}}{2}, \tag{14}$$

where $C_1=\frac{1}{2}(\Delta-i\Gamma_x)$, $C_2=\frac{1}{2}(\Delta+i\Gamma_y)$, and $\beta=\sqrt{\beta_x\beta_y}$. We first consider the resonant case where $\Delta=0$, with the x mode acting as a linearly damped oscillator and the y mode acting as an oscillator with linear gain. The variation of the eigenvalues with coupling strength for this case is presented in Fig. 2. It can be seen from Figs. 2(a) and 2(b) that, for the parametric regime where $\beta>\gamma/2$ with $\gamma_{gx}=\gamma_{gy}=\gamma$, and $\gamma_{ay}=2\gamma$, the imaginary parts of both the eigenvalues are zero, while the real parts are nonzero, depicting a $\mathcal{PT}$-symmetric behavior [44]. Further, for the nonresonant case $\Delta\neq 0$, the imaginary part of the eigenvalue is nonzero as shown in Fig 2(c), depicting the system to be in a broken-$\mathcal{PT}$-symmetric regime. This is due to the fact that, in the nonresonant case, the energy transfer between the x mode and the y mode is unbalanced [29]. Next, in order to have a better understanding of this $\mathcal{PT}$-symmetric behavior, we study the dynamics of the oscillator x and y modes using Eqs. (7)–(10). The solution for the complex amplitude for both the modes is given as

$$a_x(t)=\frac{a_0}{2\Gamma_s}e^{-\frac{(\Gamma_x+\Gamma_y+i\Gamma_s)t}{4}}\big[\Gamma_s\big(e^{\frac{i\Gamma_st}{2}}+1\big)+(i\Gamma_x-i\Gamma_y-2\Delta-4\omega_3)\big(e^{\frac{i\Gamma_st}{2}}+1\big)\big], \tag{15}$$

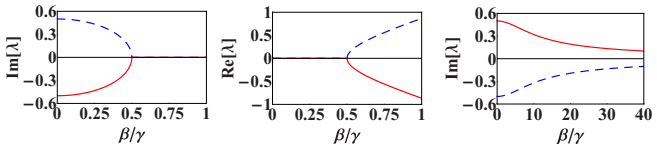

FIG. 2. $\mathcal{PT}$ symmetry in the coupled-mode levitated nanoparticle system. Panels (a) and (b) respectively show the variation of the imaginary and real parts of the eigenvalues λ_+(blue dashed line) and λ_-(red solidline) [see Eqs. (14)] with coupling strength β for $\Delta = 0$ Hz. Panel (c) shows the variation for the imaginary part of eigenvalues for $\Delta = 1.0$ Hz. Parameters are $\omega_x = 2\pi \times 115$ KHz, $\omega_y = 2\pi \times 141$ KHz, $\gamma_{gx} = \gamma_{gy} = \gamma = 2\pi \times 10$ mHz, $\gamma_{ay} = 4\pi \times 10$ mHz, and $\gamma_{cx} = \gamma_{cy} = 0.0$ Hz. Experimental values of the parameters are taken from Ref. [39].

$$a_y(t) = \frac{a_0}{2\Gamma_s} e^{-\frac{(\Gamma_x+\Gamma_y+i\Gamma_s)t}{4}} [\Gamma_s(e^{\frac{i\Gamma_s t}{2}} + 1) + (-i\Gamma_x + i\Gamma_y + 2\Delta - 4\omega_3)(e^{\frac{i\Gamma_s t}{2}} + 1)], \quad (16)$$

where $\Gamma_s = \sqrt{[2\Delta - i(\Gamma_x - \Gamma_y)]^2 + (4\omega_3)^2}$ and a_0 is the initial amplitude for the modes. At first, we probe the dynamics of the oscillator modes in the uncoupled state considering equal gain and loss values. The analytical solutions for this case ($\gamma_{gx} = \gamma_{gy} = \gamma$ and $\gamma_{ay} = 2\gamma$) for the x and y modes are $a_x(t) = a_0 e^{-\gamma t}$ and $a_y(t) = a_0 e^{\gamma t}$, respectively. It is evident from these solutions that, in the uncoupled state, the amplitude of oscillation for the x mode decreases, depicting a damped oscillator, while for the y mode it increases, representing an oscillator with gain. Figures 3(a) and 3(d) depict the behavior of oscillator displacements for the x mode and the y mode, respectively.

Next, to observe $\mathcal{PT}$ symmetry in the coupled system, we now couple the x and y modes having equal gain and loss values, which can be arranged experimentally. We first consider the resonant case with $\Delta = 0$. In this case, the solutions of the complex amplitude for both the modes are given as

$$a_x(t) = \frac{a_0 e^{-\frac{it\sqrt{\alpha}}{2}}}{4\sqrt{\alpha}} [(2i\gamma + 2\sqrt{\alpha} - 4\omega_3)e^{it\sqrt{\alpha}} + (-2i\gamma + 2\sqrt{\alpha} + 4\omega_3)], \quad (17)$$

$$a_y(t) = \frac{a_0 e^{-\frac{it\sqrt{\alpha}}{2}}}{4\sqrt{\alpha}} [(-2i\gamma + 2\sqrt{\alpha} - 4\omega_3)e^{it\sqrt{\alpha}} + (2i\gamma + 2\sqrt{\alpha} + 4\omega_3)], \quad (18)$$

where $\alpha = 4\omega_3^2 - \gamma^2$. It is apparent from Eqs. (17) and (18) that both the modes show sustained oscillation only when $\alpha > 0$ or else the oscillation increases exponentially. The condition $\alpha > 0$ is equivalent to the condition $\beta > \gamma/2$ which is discussed above and represents the condition for observing $\mathcal{PT}$ symmetry in the coupled system. Further, this parameter regime ensures that the Hamiltonian of the system has real eigenvalues [44]. Under these conditions, as expected, the coupled system shows $\mathcal{PT}$-symmetric behavior resulting in a periodic (Rabi) oscillation of mean position for both the oscillator modes with constant amplitude as depicted in Figs. 3(b) and 3(e). However, when we consider the nonresonant case with $\Delta \neq 0$, we see from Figs. 3(c) and 3(f) that the oscillation in both the modes increases exponentially even in the parametric regime of $\beta > \gamma/2$. As explained earlier, this is due to unbalanced energy transfer between the two transverse modes. Hence, in order to observe $\mathcal{PT}$ symmetry in this coupled system, it is necessary to work in the resonant regime with $\Delta = 0$.

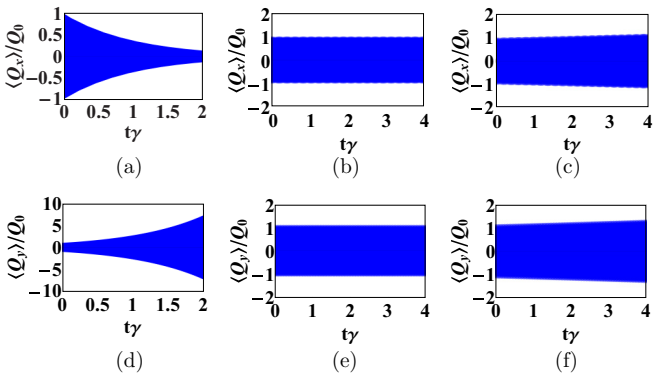

FIG. 3. The evolution of oscillation amplitudes for a coupled-mode levitated nanoparticle. Panels (a)–(c) show the dynamics of the x mode and panels (d)–(f) show the dynamics for the y mode, respectively. Parameters for panels (a) and (d) are $\delta = 0$, for panels (b) and (e) are $\delta = 10^{-4}$ and $\Delta = 0$ Hz, and for panels (c) and (f) are $\delta = 10^{-4}$ and $\Delta = 1$ Hz. The remaining parameters are $\omega_x = 2\pi \times 115$ KHz, $\omega_y = 2\pi \times 141$ KHz, $\gamma_{gx} = \gamma_{gy} = \gamma = 2\pi \times 10$ mHz, $\gamma_{ay} = 4\pi \times 10$ mHz, $\gamma_{cx} = \gamma_{cy} = 0.0$ Hz, $Q_0 = \sqrt{4 \times 10^5}$, and $T = 1$ K. Experimental values of the parameters are taken from Ref.[39].

Recently, similar results on $\mathcal{PT}$-symmetric dynamics in clamped optomechanical system have been presented by Xu *et al.* [45]. Comparing with the work by Xu *et al.* [45], our result do have mathematical similarity between the equation of motion in the linear regime and, hence, similar $\mathcal{PT}$-symmetric dynamics; however, there are several important physical differences between our work and theirs. First, we present a model based on cavityless levitated optomechanics, which is fundamentally different from the model by Xu *et al.* [45] which involves a passive cavity. Second, the coupling in our work is initiated between two mechanical modes, while in the work by Xu *et al.* [45], it is between an optical mode and a mechanical mode. Although all modes involved in both works are bosonic, there is a large difference between the parameters (such as mode frequencies and phonon and photon numbers) and physical behavior (e.g., massive versus massless, localized versus traveling at the speed of light, and damping mechanisms). Third, we not only study $\mathcal{PT}$ symmetry in the linear regime but also use this phenomena to look for the possibility of achieving lasing action in the coupled system, which makes our analysis different from the work of Xu *et al.* [45].

Moreover, we also demonstrate $\mathcal{PT}$ symmetry in the nonlinear regime. Nonlinear $\mathcal{PT}$ symmetry is an interesting phenomena in which a system shows stable dynamics even in the regime where the $\mathcal{PT}$ condition is not satisfied and has been used to study bistability and bifurcations in nonlinear coupled systems [46]. In addition to this, we also look for the possible application towards utilizing the coupled levitated

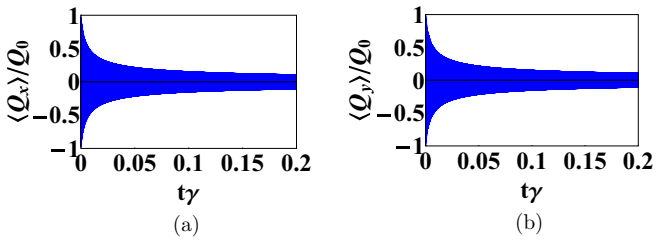

FIG. 4. Position dynamics of the x mode (a) and the y mode (b) in the nonlinear $\mathcal{PT}$-symmetric regime. The parameters are $\omega_x = 2\pi \times 115$ KHz, $\omega_y = 2\pi \times 141$ KHz, $\gamma_{gx} = \gamma_{gy} = \gamma = 2\pi \times 10$ mHz, $\gamma_{ay} = 4\pi \times 10$ mHz, $\gamma_{cx} = \gamma_{cy} = 10^{-5}$ Hz, $\Delta = 0$ Hz, $\delta = 10^{-3}$, $Q_0 = \sqrt{4 \times 10^5}$, and $T = 1$ K.

system in a nonlinear $\mathcal{PT}$-symmetric regime to achieve phonon lasing. These additional analyses on nonlinear $\mathcal{PT}$ symmetry and its applicability to phonon lasing distinguish our work from that of Xu *et al.* [45].

In order to investigate $\mathcal{PT}$ symmetry in the nonlinear regime, we consider the full dynamical equation for the amplitudes a_x and a_y as in Eqs. (9) and (10) which includes the nonlinear feedback terms corresponding to γ_{cx} and γ_{cy}. In the parameter regime $\gamma_{gx} = \gamma_{gy} = \gamma$, $\gamma_{ay} = 2\gamma$, and $\gamma_{cx} = \gamma_{cy} = \gamma_n$, the equations of motion for both the modes are then expressed as

$$\langle \dot{a}_x \rangle = -\frac{i}{2}\Delta\langle a_x\rangle - \frac{1}{2}\left[\gamma + 3\gamma_n\langle a_x^2\rangle\right]\langle a_x\rangle + i\beta_x\langle a_y\rangle, \quad (19)$$

$$\langle \dot{a}_y \rangle = i\beta_y\langle a_x\rangle + \frac{i}{2}\Delta\langle a_y\rangle - \frac{1}{2}\left[-\gamma + 3\gamma_n\langle a_y^2\rangle\right]\langle a_y\rangle. \quad (20)$$

The above equations closely resemble the equation for coupled nonlinear Schrödinger dimers [46]. We now numerically solve the above equations of motion to study the position dynamics of both the modes; the results are shown in Fig. 4. It is observed that the position dynamics of both modes attain a steady value in the long interaction time limit. The values for the amplitude of oscillation in this limit can be obtained by solving Eqs. (19) and (20) in the steady state, i.e., by considering $\langle \dot{a}_x \rangle = \langle \dot{a}_y \rangle = 0$. In the steady state, for $\Delta = 0$ and $\gamma \neq 0$, the dimer equations, Eqs. (19) and (20), have two solutions, notably symmetric ($a_x = a_y = a$) and antisymmetric ($a_x = -a_y = b$). These two stationary solutions are given as

$$a = [\sqrt{4\beta^2 - \gamma^2}/(3\gamma_n)]^{1/2} e^{i(\theta_1 + \frac{\pi}{2})}, \quad (21)$$

$$b = [\sqrt{4\beta^2 - \gamma^2}/(3\gamma_n)]^{1/2} e^{i\theta_2}, \quad (22)$$

where $\sin(\theta_2 - \theta_1) = -\gamma/(2\beta)$ [46]. From the above analysis, it is evident that the system shows sustained oscillation in the long interaction time limit and, hence, can be considered to be in the nonlinear $\mathcal{PT}$-symmetric regime [46] represented by $\Delta = 0$ and $\beta > \gamma/2$. A more detailed analysis on the dynamics of the dimer equation can be found in Ref. [47].

Moreover, when the system is sufficiently cooled down, the noise terms in Eqs. (3)–(6) play an important part and should be taken into account [10]. Following our theoretical demonstration of $\mathcal{PT}$ symmetry in both linear and nonlinear regimes in this levitated system, this model can be realized experimentally and be utilized to further explore phenomena

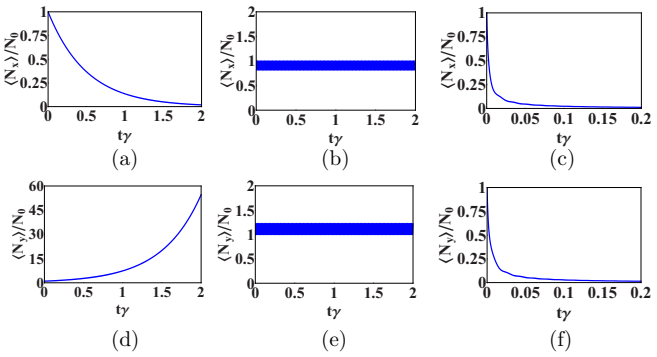

FIG. 5. The time evolution of the phonon population for a coupled-mode levitated nanoparticle. Panels (a) and (b) show the phonon dynamics of the x mode in the linear $\mathcal{PT}$-symmetric regime for $\delta = 0$ and $\delta = 10^{-4}$, respectively, with $\Delta = 0$ Hz. Panels (d) and (e) show the dynamics of the y mode also in the linear $\mathcal{PT}$-symmetric regime for $\delta = 0$ and $\delta = 10^{-4}$, respectively, for $\Delta = 0$ Hz. Panels (c) and (f) show the phonon dynamics for the x mode and the y mode, respectively, in the nonlinear $\mathcal{PT}$-symmetric regime with $\delta = 10^{-4}$, $\gamma_{cx} = \gamma_{cy} = 10^{-5}$ Hz, and $\Delta = 0$ Hz. Here $N_0 = 2 \times 10^5$, while other parameters are the same as those in Fig. 3.

such as $\mathcal{PT}$-symmetric phonon laser [30], squeezing enhancement [31], generation of nonclassical states [32], and efficient entanglement [48] and for studying nonlinear dynamics in coupled many-body system [49].

In particular, we are interested in the possibility of realizing a $\mathcal{PT}$-symmetric phonon laser in this system. Hence, we now investigate if the sustained oscillation showed by the system in the linear and nonlinear $\mathcal{PT}$-symmetric regimes can be linked to lasinglike behavior. For this, we first study the phonon dynamics as well as the second-order coherence for the coupled-mode system in the linear $\mathcal{PT}$-symmetric regime. In the classical limit, the phonon dynamics can be well represented by $|a_x(t)|^2$ for x mode and $|a_y(t)|^2$ for y mode, respectively. In the uncoupled state, with equal gain and loss value, the evolution of phonon population in both x and y modes is represented by the forms $N_x(t) = |a_x(t)|^2 = N_0 e^{-2\gamma t}$ and $N_y(t) = |a_y(t)|^2 = N_0 e^{2\gamma t}$, respectively. It is clear from these analytical expressions that, in the absence of coupling, the phonon population for the x mode decays exponentially, while it rises for the y mode [see Figs. 5(a) and 5(d), respectively]. This is simply due to the fact that, in the uncoupled state, the x mode acts as a damped oscillator, while the y mode acts as an amplified oscillator.

Further, when both the modes are coupled, the analytical solutions for the phonon population in the two transverse modes are given as

$$N_x(t) = \frac{N_0}{2\alpha}\left[8\omega_3^2 - (\gamma^2 - i\gamma\sqrt{\alpha})e^{it\sqrt{\alpha}} - (\gamma^2 + i\gamma\sqrt{\alpha})e^{-it\sqrt{\alpha}}\right], \quad (23)$$

$$N_y(t) = \frac{N_0}{2\alpha}\left[8\omega_3^2 - (\gamma^2 + i\gamma\sqrt{\alpha})e^{it\sqrt{\alpha}} - (\gamma^2 - i\gamma\sqrt{\alpha})e^{-it\sqrt{\alpha}}\right], \quad (24)$$

where $N_0 = |a_0|^2$ is the initial phonon number. It is evident from Eqs. (23) and (24) that for $\alpha > 0$ ($\mathcal{PT}$ condition),

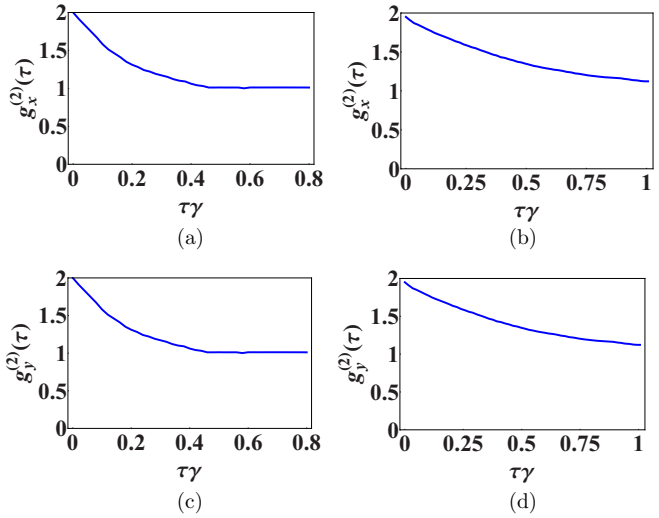

FIG. 6. Variation of second-order coherence with scaled time delay for the $\mathcal{PT}$-symmetric system. Panels (a) and (b) show $g_x^{(2)}(\tau)$ for the x mode in the linear and the nonlinear $\mathcal{PT}$-symmetric regime, respectively. Panels (c) and (d) show $g_y^{(2)}(\tau)$ for the y mode in the linear and the nonlinear $\mathcal{PT}$-symmetric regime, respectively. Corresponding parameters for each regime are the same as those in Figs. 3 and 4.

the phonon dynamics for both the modes shows oscillatory behavior, which also can been seen in Figs. 5(b) and 5(e). This sustained oscillation in the phonon dynamics is due to the fact that the mean phonon number N is proportional to the square of the mean position Q ($\langle N\rangle \propto \langle Q^2\rangle$). Now, in the $\mathcal{PT}$-symmetric regime, the position dynamics of both the modes shows sustained oscillation. Hence, in this regime, the phonon number dynamics for both the modes also have sustained oscillation. From the above study, it is apparent that the $\mathcal{PT}$-symmetric system does not show a saturationlike behavior in the phonon dynamics [28], which is one of the criteria for validating lasing action. Hence, the self-sustained oscillation of the $\mathcal{PT}$-symmetric system in the linear regime cannot be linked to lasinglike phenomena.

In order to further verify our conclusion, we also study the second-order coherence for the $\mathcal{PT}$-symmetric system in the linear regime. In this regard, we solve Eqs. (7)–(10) using the numerical method in Refs. [50,51]. In the numerical evaluation process, at each time step, we find the position (Q_j) and momentum (P_j) values and then add the noise term as in Eqs. (3)–(6) to the momentum (P_j) values. Next, from the modified Q_j and P_j, we find the modified complex amplitudes a_x and a_y. We then use the new a_x and a_y as the initial condition and solve Eqs. (9) and (10) for the next time step, and we follow the same procedure to find the full solution for a_x and a_y in the presence of noise. Later, we use these complex amplitude values to find the second-order coherence as in Eq. (11), the result of which is shown in Fig. 6. It is evident from Figs. 6(a) and 6(c) that $g_x^{(2)}(\tau)$ and $g_y^{(2)}(\tau)$ for both the modes show a Lorentzian-type feature indicating that both modes are in the thermal state [52].

Next, we proceed to study the phonon dynamics and the second order coherence for the coupled system in the nonlinear $\mathcal{PT}$-symmetric regime. In this regime, the system have a steady value of population in both modes in the long interaction time limit as shown in Figs. 5(c) and 5(f), and the value of which can be evaluated either by $|a|^2$ or by $|b|^2$ from Eqs. (21) and (22). However, though the system have stable phonon population, the test of second-order coherence as depicted in Figs. 6(b) and 6(d) still shows both modes to be in thermal state.

Hence, from the above studies of phonon dynamics as well as the second-order coherence, it appears that lasinglike phenomena in the system remain inaccessible when the system is in either the linear or the nonlinear $\mathcal{PT}$-symmetric regime. However it may be possible to attain simultaneous lasing action in such a gain-loss system by working in a nonlinear regime considering the value of gain to be very much higher than that of loss [53,54]. The presence of such high gain along with nonlinearity in a mode drives the corresponding mode towards lasing [28]. Coherent coupling of any nonlasing mode to this lasing mode can then induce lasing in the former mode. In the next section, we present a detailed discussion of this induced lasing mechanism and also discuss how the presence and the absence of the nonlinearity in the modes affect this mechanism.

B. Lasing transfer and creation

In this subsection, we demonstrate coupling-induced lasing transfer between the two transverse modes of the levitated nanoparticle, prepared in various initial configurations. Apart from this, we also show coupling-induced simultaneous lasing of the transverse modes via nonlinear feedback, when neither of them show lasing action initially. At first, we consider the x mode as a nonlinearly damped oscillator, i.e., the x mode is subjected to nonlinear feedback cooling [40], and the y mode as a phonon laser which requires both amplification and cooling [28]. The initial configuration for both the modes are characterized by studying the position dynamics, the phonon dynamics, and the second-order coherence. In this regard, we first study the position dynamics for both the modes of the coupled system using Eqs. (9) and (10). For the uncoupled case, we can write the approximate analytical solutions for both the modes as

$$a_x(t) = a_0 \frac{\sqrt{\gamma_{gx}}}{\sqrt{e^{2\gamma_{gx}(t+\theta_1)} - 6a_0^2\gamma_{cx}}}, \tag{25}$$

$$a_y(t) = a_0 \frac{\sqrt{\gamma_{gy} - \gamma_{ay}}}{\sqrt{e^{2(\gamma_{gy}-\gamma_{ay})(t+\theta_2)} - 6a_0^2\gamma_{cy}}}, \tag{26}$$

where $\theta_1 = \ln[6a_0^2\gamma_{cx} + \gamma_{gx}]/2\gamma_{gx}$ and $\theta_2 = \ln[6a_0^2\gamma_{cy} + \gamma_{gy} - \gamma_{ay}]/[2(\gamma_{gy} - \gamma_{ay})]$.

It is clear from the above solutions, and as expected, that the x mode simply damps, while the y mode initially shows exponential rise and then saturates to a higher amplitude ($\approx \sqrt{\gamma_{ay}/\gamma_{cy}}$) as shown in Figs. 7(a) and 7(d), respectively. Further, Eqs. (26) reveals that the nonlinear cooling term γ_{cy} plays an important role in attaining the saturation value in the amplitude of the y mode. The competition between nonlinear feedback cooling γ_{cy} and linear heating γ_{ay} is the basic phenomenon behind the attainment of such a saturation value and, hence, the cause of lasing in the y mode.

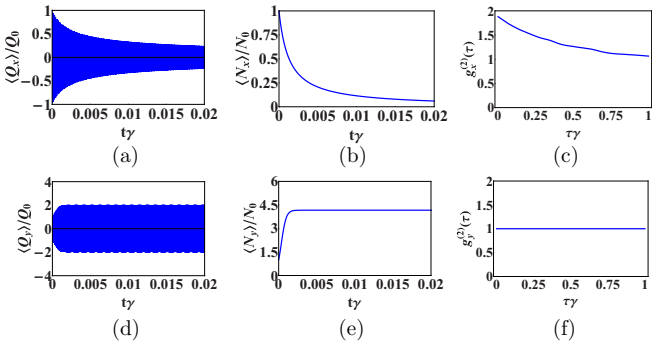

FIG. 7. Initial configuration of the coupled-mode levitated system. Panels (a)–(c) show the position dynamics, the phonon dynamics, and the second-order coherence for the x mode, respectively. Panels (d)–(f) show the position dynamics, the phonon dynamics, and the second-order coherence for the y mode, respectively. The parameters are $\omega_x = 2\pi \times 115$ KHz, $\omega_y = 2\pi \times 141$ KHz, $\gamma_{gx} = \gamma_{gy} = \gamma = 2\pi \times 10$ mHz, $\gamma_{cx} = 10^{-5}$ Hz, $\gamma_{cy} = 10^{-5}$ Hz, $\Gamma_{cx} = 10^{-6}$ Hz, $\Gamma_{cy} = 10^{-6}$ Hz, $\gamma_{ay} = 100$ Hz, $\delta = 0$, $\Delta = 0$ Hz, $Q_0 = \sqrt{4 \times 10^5}$, $N_0 = 2 \times 10^5$, $A_{tx} = A_{ty} = 1$ KHz, $D_{px} = D_{py} = 24$ KHz, $D_x = D_y = 5 \times 10^{-8}$ Hz, and $T = 1$ K. Experimental values of the parameters are taken from Refs. [28,39].

Further, the phonon dynamics for the modes can be studied numerically by solving Eqs. (9) and (10). The evolution of the phonon population for x and y modes is then evaluated from $N_x(t) = |a_x(t)|^2$ and $N_y(t) = |a_y(t)|^2$, respectively, and the result is shown in Fig. 7. It is evident from Figs. 7(b) and 7(e), respectively, and also can be predicted from the analytical expressions in Eqs. (25) and (26), that the phonon population in the x mode decays, while for the y mode the phonon population shows a saturation effect with a value ($\approx \gamma_{ay}/\gamma_{cy}$) (previously observed in Ref. [28]).

We also study the second-order coherence for both the modes, which is evaluated using the same procedure as discussed above in the $\mathcal{PT}$ symmetry section (Sec. III A). Figures 7(c) and Fig. 7(f) show the behavior of second-order coherence $g_x^{(2)}(\tau)$ for the x mode and $g_y^{(2)}(\tau)$ for the y mode, respectively. It is seen in the figure that $g_x^{(2)}(\tau)$ has a Lorentzian profile depicting the mode to be in a thermal state and $g_y^{(2)}(\tau)$ has a constant profile representing it to be in a coherent state [42]. The above analysis confirms that the x mode acts as a damped oscillator and the y mode acts as a phonon laser, which is expected from the initial condition. Next, we use this analysis to establish lasing transfer in the coupled case as well.

In this regard, we first study the position dynamics of the x mode and the y mode, when both the modes are coupled, the results of which are shown in Figs. 8(a) and 8(d), respectively. Figure 8(a) shows that, when the modes are coupled, the y mode induces a sustained oscillation in the x mode (which was initially a nonlinearly damped oscillator). Further, to check that the sustained oscillation of the x mode indeed leads to lasing of the mode, we study the phonon dynamics for the coupled system. Figure 9(a) shows the phonon dynamics for the x mode in the presence of coupling. It is apparent from the figure that the phonon population in the x mode attains a saturation value, which points to a lasinglike phenomenon, indicating lasing transfer to the x mode.

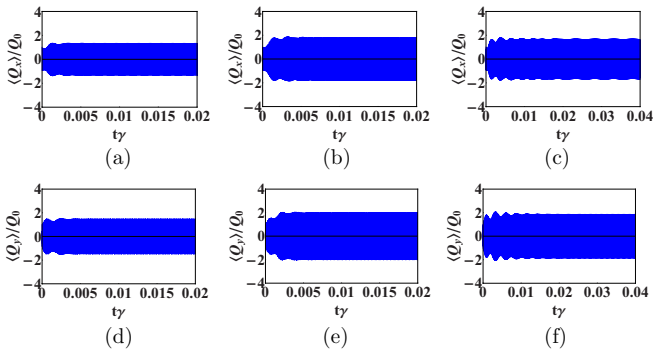

FIG. 8. Induced lasing transfer and creation in a coupled-mode levitated system. Panels (a)–(c) show the position dynamics of the x mode and panels (d)–(f) show the position dynamics for the y mode, for $\delta = 10^{-3}$. The parameters for panels (a) and (d) are $\gamma_{cx} = 10^{-5}$ Hz and $\gamma_{cy} = 10^{-5}$ Hz. The parameters for panels (b) and (e) are $\gamma_{cx} = 0$ Hz, $\gamma_{cy} = 10^{-5}$ Hz. For panels (c) and (f), the parameters are $\gamma_{cx} = 10^{-5}$ Hz, $\gamma_{cy} = 0$ Hz, and $\gamma_{ay} = 70$ Hz. Other parameters are the same as those in Fig. 7.

Next, to fully establish this induced lasing transfer, we also study the second-order coherence for the x mode, the results of which are shown in Fig. 10. It can be seen from Fig. 10(a) that, with the introduction of coupling in the system, $g_x^{(2)}(\tau)$ for the x mode shows a constant profile, which initially had a Lorentzian profile, indicating that the mode has evolved to a coherent state. Hence, our study of both the phonon dynamics and the second-order coherence confirms the induced lasing transfers between the modes in the coupled system. Now, as for the y mode, it can be seen from Figs. 8(d) and 9(d) that the amplitude of oscillation and the phonon population slightly decrease while preserving the sustained oscillation and saturation effect in the mode. This decrease in both oscillation amplitude and phonon population is due to the coupling of the y mode to the nonlinearly damped x mode, which induces extra damping in the y mode. Further, $g_y^{(2)}(\tau)$ for the y mode

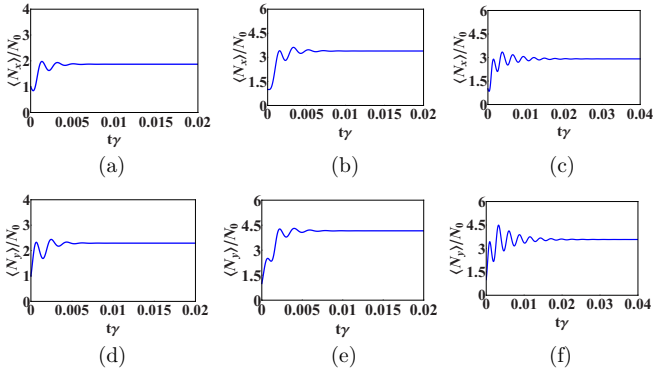

FIG. 9. Saturation effect in phonon dynamics for the coupled-mode levitated system. Panels (a)–(c) show the phonon dynamics of the x mode and panels (d)–(f) show the phonon dynamics for the y mode, for $\delta = 10^{-3}$. The parameters for panels (a) and (d) are $\gamma_{cx} = 10^{-5}$ Hz and $\gamma_{cy} = 10^{-5}$ Hz. The parameters for panels (b) and (e) are $\gamma_{cx} = 0$ Hz and $\gamma_{cy} = 10^{-5}$ Hz. For panels (c) and (f), the parameters are $\gamma_{cx} = 10^{-5}$ Hz, $\gamma_{cy} = 0$ Hz, and $\gamma_{ay} = 70$ Hz. Other parameters are the same as those in Fig. 7.

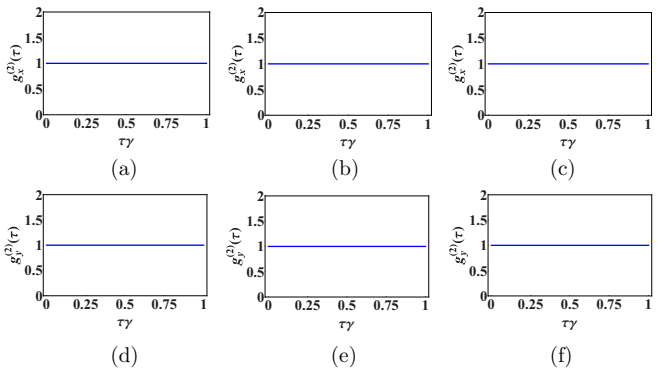

FIG. 10. The second-order coherence as a function of scaled time delay for the coupled-mode levitated system. Panels (a)–(c) show $g_x^{(2)}(\tau)$ for the x mode and panels (d)–(f) show $g_y^{(2)}(\tau)$ for the y mode, respectively. Parameters for panels (a) and (d) are $\gamma_{cx} = 10^{-5}$ Hz and $\gamma_{cy} = 10^{-5}$ Hz. Parameters for panels (b) and (e) are $\gamma_{cx} = 0$ Hz and $\gamma_{cy} = 10^{-5}$ Hz. Parameters for panels (c) and (f) are $\gamma_{cx} = 10^{-5}$ Hz, $\gamma_{cy} = 0$ Hz, and $\gamma_{ay} = 70$ Hz. Other parameters are the same as those in Fig 8.

as in Fig. 10(d) depicts that the state of the y mode remains unchanged; i.e., it is still in the coherent state even after coupling.

Next, we consider the case when no nonlinear feedback cooling ($\gamma_{cx} = 0$) is applied to the x mode; i.e., the mode acts as a linearly damped oscillator, while the y mode is considered as a phonon laser. We then introduce the coupling and analyze the possibility of attaining induced lasing in the x mode for this case. In this regard, we study the position dynamics, the phonon dynamics, and the second-order coherence for the x mode. Now, when the coupling is in effect, it can be seen from Fig. 8(b) that the linearly damped x mode shows sustained oscillation. Further, the phonon population for the x mode also attains a saturation value as shown in Fig. 9(b). Both of these results indicate induced lasing transfer in the x mode, which is further established from $g_x^{(2)}(\tau)$ as in Fig. 10(b), showing the mode to be in a coherent state. Moreover, in this case the state of the y mode remains unchanged as can be seen from Figs. 9(e) and 10(e). Hence, from the above analysis, we can affirm that both linear and nonlinear damped oscillator modes achieve induced lasing when coupled to a phonon laser.

At last, we discuss the case where initially the x mode acts as a nonlinearly damped oscillator, while the y mode acts a linear gain oscillator ($\gamma_{cy} = 0$). We then couple both the modes and discuss the possibility of achieving simultaneous lasing in the modes. For this, we study the dynamics of position and the phonon population along with the second-order coherence for both the modes. When the modes are coupled, it can be seen from Figs. 8(c) and 8(f) that the position dynamics show sustained oscillation for both x and y modes, respectively. As a result, the phonon dynamics for both x and y modes also attain saturation as seen in Figs. 9(c) and 9(f), respectively. These results represent that both the modes have attained simultaneous lasing due to this coupling.

Further, we confirm the induced lasing action from $g_x^{(2)}(\tau)$ and $g_y^{(2)}(\tau)$, which shows both x and y modes to be in a coherent state as seen in Figs. 10(c) and 10(f), respectively. The induced lasing action in both the modes can be attributed to the competition between linear amplification in the y mode and nonlinear damping in the x mode [28]. All the above analysis on lasing transfer and simultaneous lasing is done for the resonant case $\Delta = 0$, and we find that these results remain unchanged even for the nonresonant case $\Delta \neq 0$. Simultaneous lasing in all directions is very much essential as it might have applications in imaging using coherent phonons [36]. Apart from this, the above presented results can stimulate studies on outcoupling of phonon lasers and obtaining high-fidelity quantum state transfer [33] as well as efficient synchronization [34,55], which have potential applications in quantum information processing [37].

C. Force sensing

In this section, we study force sensing using a coupled-mode levitated nanoparticle. In order to calculate the force sensitivity, we consider both the modes as a nonlinearly damped oscillator and write the equations of motion for the coupled-mode system as

$$\ddot{q}_x = -\omega_x^2 q_x - \frac{\kappa\delta}{m}\cos(\omega_r t) q_y - 2[\gamma_{gx} + 3\gamma_{cx}(2\langle N_x\rangle + 1)]\dot{q}_x + \frac{F_x}{m}, \tag{27}$$

$$\ddot{q}_y = -\omega_y^2 q_y - \frac{\kappa\delta}{m}\cos(\omega_r t) q_x - 2[\gamma_{gy} + 3\gamma_{cy}(2\langle N_y\rangle + 1)]\dot{q}_y + \frac{F_y}{m}, \tag{28}$$

where $F_j = F_T^j + F_{\mathrm{Fa}}^j + F_{\mathrm{Fc}}^j$, $F_T^j = \sqrt{2K_B T m\gamma_{gj}}\xi_T$, $F_{\mathrm{Fa}}^j = \sqrt{D_{tj}\hbar\omega_j m}\xi_{\mathrm{Fa}}$, and $F_{\mathrm{Fc}}^j = 12q_j^2\sqrt{\frac{\Gamma_{cj}^2 m^3\omega_j^3}{\hbar\gamma_{cj}}}\xi_{\mathrm{Fc}}$, with $j \in \{x, y\}$. Next, we solve the above equations in the Fourier domain and express the solutions in the forms $q_x(\omega) = \chi_x(\omega)F_x(\omega)$ and $q_y(\omega) = \chi_y(\omega)F_y(\omega)$, where $\chi_x(\omega)$ and $\chi_y(\omega)$ are the optomechanical susceptibilities for the x and y modes, respectively. The susceptibilities for the modes are given as

$$\chi_j(\omega) = \frac{1 + A_v(\omega) + B_v(\omega)}{m[(\omega_j^2 - \omega^2) + i\omega\Gamma_j]} \quad \text{for } j \neq v, \tag{29}$$

$$A_v(\omega) = \frac{\kappa\delta}{2m\{[\omega_v^2 - (\omega - \omega_r)^2] + i(\omega - \omega_r)\Gamma_v\}}, \tag{30}$$

$$B_v(\omega) = \frac{\kappa\delta}{2m\{[\omega_v^2 - (\omega + \omega_r)^2] + i(\omega + \omega_r)\Gamma_v\}}, \tag{31}$$

where both j and $v \in \{x, y\}$. A detailed analysis of the above derivation is provided in the Appendix. We now include the effect of the shot noise of the measured signal and write the positional power spectral density (PSD) for both the modes as

$$\langle|q_j(\omega)|^2\rangle = |\chi_j(\omega)|^2(S_{Tj} + S_{Hj} + S_{Cj}) + \frac{l_j^2}{\eta^2\phi}, \tag{32}$$

where η and ϕ are the optomechanical coupling coefficient and the photon flux [40], respectively, and $l_j = \sqrt{\hbar/2m\omega_j}$ is the oscillator length, along with $j \in \{x, y\}$. Further, the stochastic forces due to thermal heating, feedback heating, and feedback cooling are given as $S_{Ti} = 2m\gamma_{gj}K_B T$,

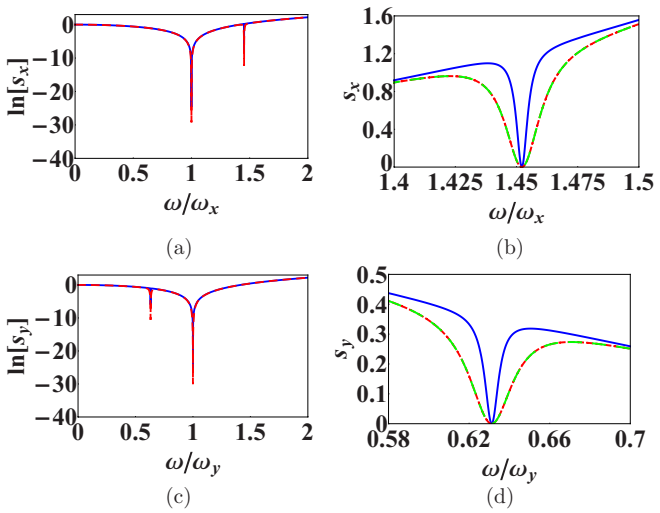

FIG. 11. Shot noise force PSD as a function of frequency. Panels (a) and (d) respectively show $\ln[s_x]$ with $s_x = S_{sx}(\omega)/S_{s0}$ of the x mode and $\ln[s_y]$ with $s_y = S_{sy}(\omega)/S_{s0}$ of the y mode, for $\delta = 10^{-5}$ (blue solid lines) and $\delta = 10^{-3}$ (red dashed lines). Panels (b) and (d) respectively show the enlarged view of the second minimum of $S_{sx}(\omega)/S_{s0}$ and $S_{sy}(\omega)/S_{s0}$ for $\delta = 10^{-4}$, $\gamma_{cx} = 10^{-4}$ Hz, $\gamma_{cy} = 10^{-4}$ Hz (blue solid lines); $\delta = 10^{-3}$, $\gamma_{cx} = 10^{-4}$ Hz, $\gamma_{cy} = 10^{-4}$ Hz (red dot-dashed lines); and $\delta = 10^{-3}$, $\gamma_{cx} = 10^{-5}$ Hz, $\gamma_{cy} = 10^{-5}$ Hz (green dashed lines). The parameters are $\omega_x = 2\pi \times 115$ KHz, $\omega_y = 2\pi \times 141$ KHz, $\gamma_{gx} = \gamma_{gy} = \gamma = 2\pi \times 10$ mHz, $\gamma_{cx} = 10^{-4}$ Hz, $\gamma_{cy} = 10^{-4}$ Hz, $\Gamma_{cx} = 10^{-5}$ Hz, $\Gamma_{cy} = 10^{-5}$ Hz, $\gamma_{ay} = 0$ Hz, $A_{tx} = 10$ KHz, $A_{ty} = 10$ KHz, $\eta = 2 \times 10^{-7}$, $\phi = 5 \times 10^{17}$ photons/s, $D_{px} = D_{py} = 24$ KHz, $D_x = D_y = 5 \times 10^{-8}$ Hz, and $T = 1$ K. The nanoparticle diameter $D = 136$ nm and the density $\rho = 2200\,\mathrm{kg/m^3}$. Experimental values of the parameters are taken from Refs. [39,40]. The values of stochastic forces for the parameters considered above are $S_{Tx} \approx S_{Ty} = 2 \times 10^{-42}\ \frac{N^2}{Hz}$, $S_{Hx} \approx S_{Hy} = 2.7 \times 10^{-42}\ \frac{N^2}{Hz}$, $S_{Cx} \approx S_{Cy} = 5 \times 10^{-43}\ \frac{N^2}{Hz}$, and $S_{s0} = 1.8 \times 10^{-38}\ \frac{N^2}{Hz}$.

$S_{Hj} = \hbar m \omega_j D_{tj}$, and $S_{Cj} = 36\hbar m \omega_j \frac{\Gamma_{cj}^2}{\gamma_{cj}}[4\langle N_j\rangle^2 + 4\langle N_j\rangle + 1]$, respectively.

Now from the PSD equation as in Eq. (32), we can write the force PSD for each mode as

$$\langle |F_j(\omega)|^2\rangle = S_{Tj} + S_{Hj} + S_{Cj} + S_{sj}(\omega), \tag{33}$$

where $S_{sj}(\omega) = S_{s0}/|\chi_j(\omega/\omega_j)|^2$, with $S_{s0} = m^2 l_j^2 \omega_j^4/\eta^2\phi$ and $j \in \{x, y\}$ [40].

To obtain a minimum force sensitivity, we consider the case where the frequency-dependent term $S_{sj}(\omega)$ is minimum. Hence, in this regard we numerically study $S_{sj}(\omega)$ and present the results in Fig. 11. It can be seen from Figs. 11(a) and 11(c), which apply for low values of the coupling (blue solid line), that the force PSD $[S_{sj}(\omega)]$ attains a minimum value around the oscillation frequencies for each mode. Considering optimal parameters as in Fig. 11, we find a minimum force sensitivity for the coupled system to be $\sqrt{\langle |F_j(\omega)|^2\rangle_{\min}} \approx 10^{-21} N/\sqrt{\mathrm{Hz}}$, which is similar to the sensitivity observed in other single-mode levitated systems [21,56].

However, it is interesting to notice that in the case of higher values of coupling (red dashed line), the force noise PSD for the x mode has an extra minimum at $\omega_y + \omega_r$ apart from the minimum at ω_x, while the y mode has an extra minimum at $\omega_x - \omega_r$ along with the minimum at ω_y, as shown in Figs. 11(a) and 11(c), respectively. Further, the position of the extra minimum can be tuned by changing ω_r, i.e., by changing the asymmetry of the potential in the transverse plane. In principle, the asymmetry of the trapping potential can be modulated by using either an elliptically [57] or a linearly polarized [29,58] trapping laser. The asymmetry in the potential is maximum for a linearly polarized trapping laser, which results in the maximum splitting between the eigenfrequencies of the x and y modes. For our current work, we considered a linearly polarized trapping laser as in Ref. [29] and, hence, $2\pi \times 26$ KHz is the maximum value which can be achieved for ω_r in this coupled-mode levitated system.

Apart from this, we can see from Figs. 11(b) and 11(d) that not only the position of the second minimum but also its bandwidth can be controlled by tuning the coupling strength. The bandwidths of the force noise PSD minimum for the x mode at $\omega_y + \omega_r$ and for the y mode at $\omega_x - \omega_r$ are found to be $\Delta\omega/\omega_x = 0.004$ and $\Delta\omega/\omega_y = 0.007$, respectively, for $\delta = 10^{-4}$ (blue solid line). Also, with the increase in the coupling strength, i.e., for $\delta = 10^{-3}$ (red dot-dashed line), the bandwidths of the force noise PSD for both the x mode and the y mode increases and are found to be $\Delta\omega/\omega_x = 0.014$ and $\Delta\omega/\omega_y = 0.02$, respectively.

We note that the parameter δ cannot be made arbitrarily high and has to satisfy the condition $\delta \ll 1$ for the linear approximation of the coupling as in Eq. (1) to remain valid [29]. From Figs. 11(b) and 11(d) we also see that the strength of the feedback nonlinearity does not have much effect on the bandwidths (green dashed line) of the minima for both the modes. Moreover, the presence of these extra minima suggest that the coupled-mode system can be sensitive to small forces at these extra frequencies as well. We find the minimum force sensitivity at the frequencies relevant to the secondary minima of the force noise PSD also to be $\sqrt{\langle |F_j(\omega)|^2\rangle_{\min}} \approx 10^{-21} N/\sqrt{\mathrm{Hz}}$ in the strong-coupling regime.

These features in the force PSD can be attributed to the phenomenon of mode splitting which arises generally in a coupled system and has recently been specifically experimentally identified in a levitated nanoparticle [29]. Interestingly, these results imply that one can measure weak forces at quite different frequencies with high sensitivity by tuning the coupling in the system. Hence, from the above study it is evident that the coupled-mode levitated systems are more suitable for designing tunable ultrasensitive sensors than single-mode levitated systems due to their greater tunability [35,59]. Experimentally, feedback-based in-loop protocols can be used to measure the sensitivity of such coupled systems, wherein the error in the sensitivity measurement arising due to uncertainty in position measurement and improper feedback coupling can also be accounted for [21,56,60].

IV. CONCLUSION

In conclusion, we have theoretically demonstrated $\mathcal{PT}$ symmetry, induced and simultaneous lasing, and tunable ultrasensitive force sensing in a coupled-mode levitated system. We have used quantum Langevin equations to calculate phonon evolution and second-order phonon

coherence and quantify the dynamics of the coupled system. We found that, in the regime where oscillation frequencies of both the mechanical modes as well as their strength of their coupling are very much larger than their respective damping rates, the position dynamics for both the modes show sustained modulation of oscillation, indicating $\mathcal{PT}$ symmetry.

Although the system shows oscillation with constant amplitude, the dynamics of phonon population and tests of the second-order coherence reveal both the modes to be in thermal rather than coherent states. Further, we show that the system enters a $\mathcal{PT}$-symmetric broken phase in the presence of nonresonant coupling. Next, we show that when one of the modes is in a coherent state, i.e., in a lasing mode, the other mode also attains a coherent state due to the coupling, indicating induced lasing transfer. Moreover, we have also shown coupling-induced simultaneous lasing of a nonlinearly damped mode and a linearly amplified mode. We also studied tunable force sensing in the coupled-mode levitated system and found multifrequency sensitivity of the order of $zN/\sqrt{\text{Hz}}$. Our theoretical work suggests new possibilities for an optically levitated coupled-mode nanoparticle for coherent manipulation and force sensing.

ACKNOWLEDGMENTS

This research was supported by the Office of Naval Research under Grants No. N00014-17-1-2291 and No. N00014-18-1-2370. S.S. would like to acknowledge his postdoctoral fellowship from KAIST through the BK21 project.

APPENDIX

1. Equations of motion

In the Appendix, we provide a detailed derivation of the equation of motion for the coupled modes in the mean-field approximation limit [41]. In this limit, we neglect the noise terms as in Eqs. (3)–(6) and write the equations of motion as

$$\dot{Q}_x = \omega_x P_x, \tag{A1}$$

$$\dot{P}_x = -\omega_x Q_x - 2\left(\gamma_{gx} + 3\gamma_{cx}Q_x^2\right)P_x + \frac{\kappa\delta}{m\sqrt{\omega_x\omega_y}}\cos(\omega_r t)Q_y, \tag{A2}$$

$$\dot{Q}_y = \omega_y P_y, \tag{A3}$$

$$\dot{P}_y = -\omega_y Q_y - 2\left(\gamma_{gy} - \gamma_{ay} + 3\gamma_{cy}Q_y^2\right)P_y + \frac{\kappa\delta}{m\sqrt{\omega_x\omega_y}}\cos(\omega_r t)Q_x. \tag{A4}$$

We now take the derivative of the position for the two modes as in equations Eqs. (A1)–(A4) with respect to time and obtain the following:

$$\ddot{Q}_x = -\omega_x^2 Q_x - 2\left(\gamma_{gx} + 3\gamma_{cx}Q_x^2\right)\dot{Q}_x + \frac{\kappa\delta}{m}\sqrt{\frac{\omega_x}{\omega_y}}\cos(\omega_r t)Q_y, \tag{A5}$$

$$\ddot{Q}_y = -\omega_y^2 Q_y - 2\left(\gamma_{gy} - \gamma_{ay} + 3\gamma_{cy}Q_y^2\right)\dot{Q}_y + \frac{\kappa\delta}{m}\sqrt{\frac{\omega_y}{\omega_x}}\cos(\omega_r t)Q_x. \tag{A6}$$

Next, we express the oscillation modes Q_x and Q_y in terms of their complex amplitudes as

$$Q_x = Q_0\text{Re}\{a_1(t)e^{i\omega_0 t}\}, \tag{A7}$$

$$Q_y = Q_0\text{Re}\{a_2(t)e^{i\omega_0 t}\}. \tag{A8}$$

Here $Q_0 = \sqrt{2N_0}$ is the initial amplitude of the oscillation modes, with $N_0 = \frac{k_B T}{\hbar\omega}$ as the initial phonon number at temperature T. The complex amplitudes for the oscillation modes along the x mode and the y mode are represented as a_1 and a_2, respectively. The carrier frequency of the oscillation modes is represented as $\omega_0 = \sqrt{\omega_x^2 + \omega_y^2}/2$. We then substitute Eqs. (A7) and (A8) in Eqs. (A5) and (A6) and make use of the slowly varying envelope approximation to neglect the second-order derivatives of the complex amplitudes of the modes with respect to time and write the equations of motion for the modes as

$$\dot{a}_1 = -\frac{i}{2}(\omega_1 - i\Gamma_x)a_1 - i\omega_3\sqrt{\frac{\omega_x}{\omega_y}}\cos(\omega_r t)a_2, \tag{A9}$$

$$a_2 = -i\omega_3\sqrt{\frac{\omega_y}{\omega_x}}\cos(\omega_r t)a_1 + \frac{i}{2}(\omega_1 + i\Gamma_y)a_1, \tag{A10}$$

where $\omega_1 = (\omega_y^2 - \omega_x^2)/2\omega_0$, $\Gamma_x = 2(\gamma_{gx} + 3\gamma_{cx}Q_x^2)$, $\Gamma_y = 2(\gamma_{gy} - \gamma_{ay} + 3\gamma_{cy}Q_y^2)$, and $\omega_3 = [\delta(\omega_y^2 - \omega_x^2)]/2\omega_0$. Here, we have also used the approximations $2i\omega_0 + \Gamma_x \approx 2i\omega_0$ and $2i\omega_0 + \Gamma_y \approx 2i\omega_0$ to arrive at the above equations. Further, the parameters considered in this paper for various simulations are such that this approximation is always valid. In order to further simplify the above equations of motion, we make use of following transformations:

$$a_1 = a_x(t)e^{-i\frac{\omega_r}{2}t}, \tag{A11}$$

$$a_2 = a_y(t)e^{i\frac{\omega_r}{2}t}. \tag{A12}$$

We then use the rotating-wave approximation, where we neglect the counter-rotating terms and write the final equations of motion for the mean position of the modes as

$$\langle\dot{a}_x\rangle = -\frac{i}{2}(\Delta - i\Gamma_x)\langle a_x\rangle + i\beta_x\langle a_y\rangle, \tag{A13}$$

$$\langle\dot{a}_y\rangle = i\beta_y\langle a_x\rangle + \frac{i}{2}(\Delta + i\Gamma_y)\langle a_y\rangle, \tag{A14}$$

where $\Delta = \omega_1 - \omega_r$, $\beta_x = \omega_3\sqrt{\omega_x/\omega_y}$, and $\beta_y = \omega_3\sqrt{\omega_y/\omega_x}$. Further, we also use the mean-field approximations $Q_x^2 \approx 2\langle a_x^2\rangle \approx 2\langle a_x\rangle^2$ and $Q_y^2 \approx 2\langle a_y^2\rangle \approx 2\langle a_y\rangle^2$ to express the nonlinear damping terms Γ_x and Γ_y as $\Gamma_x = 2(\gamma_{gx} + 6\gamma_{cx}\langle a_x\rangle^2)$ and $\Gamma_y = 2(\gamma_{gy} - \gamma_{ay} + 6\gamma_{cy}\langle a_y\rangle^2)$, respectively.

2. Force sensing

We consider the equations of motion as depicted by Eqs. (3)–(6) and take a derivative of the position with respect

to time for the two modes, and then we write them in the following forms:

$$\ddot{Q}_x = -\omega_x^2 Q_x - 2\left(\gamma_{gx} + 3\gamma_{cx}Q_x^2\right)\dot{Q}_x + \frac{\kappa\delta}{m}\sqrt{\frac{\omega_x}{\omega_y}}\cos(\omega_r t)Q_y + \sqrt{\frac{2K_BT\gamma_{gx}}{\hbar\omega_x}}\xi_T + \sqrt{D_{tx}}\xi_{\mathrm{Fa}} + 12Q_x^2\sqrt{\frac{\Gamma_{cx}^2}{\gamma_{cx}}}\xi_{\mathrm{Fc}}, \quad \text{(A15)}$$

$$\ddot{Q}_y = -\omega_y^2 Q_y - 2\left(\gamma_{gy} - \gamma_{ay} + 3\gamma_{cy}Q_y^2\right)\dot{Q}_y + \frac{\kappa\delta}{m}\sqrt{\frac{\omega_y}{\omega_x}}\cos(\omega_r t)Q_x + \sqrt{\frac{2K_BT\gamma_{gy}}{\hbar\omega_y}}\xi_T + \sqrt{D_{ty}}\xi_{\mathrm{Fa}} + 12Q_y^2\sqrt{\frac{\Gamma_{cy}^2}{\gamma_{cy}}}\xi_{\mathrm{Fc}}. \quad \text{(A16)}$$

We now make use of the definitions $Q_x = \sqrt{\frac{2m\omega_x}{\hbar}}q_x$ and $Q_y = \sqrt{\frac{2m\omega_y}{\hbar}}q_y$ to write the above equations of motion into their dimensional forms as

$$\ddot{q}_x = -\omega_x^2 q_x - \frac{\kappa\delta}{m}\cos(\omega_r t)q_y - 2[\gamma_{gx} + 3\gamma_{cx}(2\langle N_x\rangle + 1)]\dot{q}_x + \frac{F_x}{m}, \quad \text{(A17)}$$

$$\ddot{q}_y = -\omega_y^2 q_y - \frac{\kappa\delta}{m}\cos(\omega_r t)q_x - 2[\gamma_{gy} + 3\gamma_{cy}(2\langle N_y\rangle + 1)]\dot{q}_y + \frac{F_y}{m}, \quad \text{(A18)}$$

where $F_j = F_T^j + F_{\mathrm{Fa}}^j + F_{\mathrm{Fc}}^j$, is the net stochastic force due to thermal heating (F_T^j), feedback amplification (F_{Fa}^j), and feedback cooling (F_{Fc}^j). The stochastic forces are represented as $F_T^j = \sqrt{2K_BTm\gamma_{gj}}\xi_T$, $F_{\mathrm{Fa}}^j = \sqrt{D_{tj}\hbar\omega_j m}\xi_{\mathrm{Fa}}$, and $F_{\mathrm{Fc}}^j = 12q_j^2\sqrt{\frac{\Gamma_{cj}^2 m^3\omega_j^3}{\hbar\gamma_{cj}}}\xi_{\mathrm{Fc}}$, with $j \in \{x, y\}$. Further, in the process of achieving the above equations of motion, we considered no heating in the y mode ($\gamma_{ay} = 0$) and have used the approximations $Q_x^2 \approx (2\langle N_x\rangle + 1)$ and $Q_y^2 \approx (2\langle N_y\rangle + 1)$.

These approximations are valid for the case considered here and their validity can be verified by analyzing the phonon dynamics for both the modes in the absence and in the presence of coupling. The phonon dynamics for the modes both in the absence and in the presence of coupling are shown in Fig. 12. It is evident from the figure that the phonon dynamics for both the modes in the uncoupled state is very similar to their corresponding dynamics in the coupled case and attains

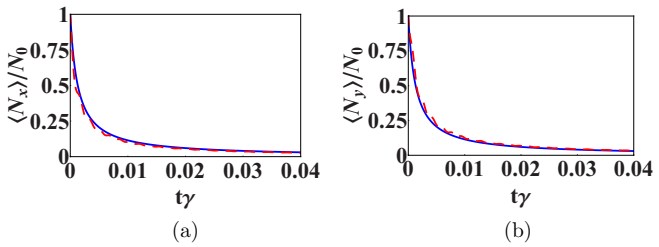

FIG. 12. Panel (a) shows the phonon dynamics for the x mode and panel (b) shows the phonon dynamics for the y mode in the absence (blue solid line) and in the presence (red dashed line) of coupling, respectively. Parameters are the same as those in Fig. 11.

a fixed value in the long time limit. Hence, in this long time interaction limit, we can safely assume $Q_x^2 \approx (2\langle N_x\rangle + 1)$ and $Q_y^2 \approx (2\langle N_y\rangle + 1)$ in our calculation [40]. We then take a Fourier transform of the above equations and rewrite them in the following forms:

$$\left[\left(\omega_x^2 - \omega^2\right) + i\omega\Gamma_x\right]q_x(\omega) + \frac{\kappa\delta}{2m}q_y(\omega - \omega_r) + \frac{\kappa\delta}{2m}q_y(\omega + \omega_r) = \frac{F_x(\omega)}{m}, \quad \text{(A19)}$$

$$\left[\left(\omega_y^2 - \omega^2\right) + i\omega\Gamma_y\right]q_y(\omega) + \frac{\kappa\delta}{2m}q_x(\omega - \omega_r) + \frac{\kappa\delta}{2m}q_x(\omega + \omega_r) = \frac{F_y(\omega)}{m}, \quad \text{(A20)}$$

where $\Gamma_x = 2[\gamma_{gx} + 3\gamma_{cx}(2\langle N_x\rangle + 1)]$ and $\Gamma_y = 2[\gamma_{gy} + 3\gamma_{cy}(2\langle N_y\rangle + 1)]$.

Next, we solve Eqs. (A19) and (A20) and write the solutions in the forms $q_x(\omega) = \chi_x(\omega)F_x(\omega)$ and $q_y(\omega) = \chi_y(\omega)F_y(\omega)$, where $\chi_x(\omega)$ and $\chi_y(\omega)$ are the optomechanical susceptibilities for the x and y modes, respectively. Here, we consider both the modes to be under nearly identical conditions, such as being subjected to the same gas damping, scattering rates, feedback rates, and temperature. Under this assumption, the mean effective forces acting on both modes can be considered to be nearly equal, i.e., $\langle|F_x(\omega)|\rangle \approx \langle|F_y(\omega)|\rangle$. In this approximation the optomechanical susceptibilities can be expressed as

$$\chi_j(\omega) = \frac{1 + A_v(\omega) + B_v(\omega)}{m[(\omega_j^2 - \omega^2) + i\omega\Gamma_j]} \quad \text{for } j \neq v, \quad \text{(A21)}$$

$$A_v(\omega) = \frac{\kappa\delta}{2m\{[\omega_v^2 - (\omega - \omega_r)^2] + i(\omega - \omega_r)\Gamma_v\}}, \quad \text{(A22)}$$

$$B_v(\omega) = \frac{\kappa\delta}{2m\{[\omega_v^2 - (\omega + \omega_r)^2] + i(\omega + \omega_r)\Gamma_v\}}, \quad \text{(A23)}$$

where both j and $v \in \{x, y\}$.

[1] H. Hodaei, A. U. Hassan, S. Wittek, H. Garcia-Gracia, R. El-Ganainy, D. N. Christodoulides, and M. Khajavikhan, Enhanced sensitivity at higher-order exceptional points, Nature (London) **548**, 187 (2017).

[2] P. Djorwe, Y. Pennec, and B. Djafari-Rouhani, Exceptional Point Enhances Sensitivity of Optomechanical Mass Sensors, Phys. Rev. Appl. **12**, 024002 (2019).

[3] Z. Zhang, Y.-P. Wang, and X. Wang, $\mathcal{PT}$-symmetry-breaking-enhanced cavity optomechanical magnetometry, Phys. Rev. A **102**, 023512 (2020).

[4] X. Mao, G.-Q. Qin, H. Yang, H. Zhang, M. Wang, and G.-L. Long, Enhanced sensitivity of optical gyroscope in a mechanical parity-time-symmetric system based on exceptional point, New J. Phys. **22**, 093009 (2020).

[5] V. Giovannetti, S. Lloyd, L. Maccone, J. H. Shapiro, and F. N. C. Wong, Conveyor-belt clock synchronization, Phys. Rev. A **70**, 043808 (2004).

[6] A. Mari, A. Farace, N. Didier, V. Giovannetti, and R. Fazio, Measures of Quantum Synchronization in Continuous Variable Systems, Phys. Rev. Lett. **111**, 103605 (2013).

[7] W. Zhang, D.-S. Ding, Y.-B. Sheng, L. Zhou, B.-S. Shi, and G.-C. Guo, Quantum Secure Direct Communication with Quantum Memory, Phys. Rev. Lett. **118**, 220501 (2017).

[8] R.-X. Chen, C.-G. Liao, and X.-M. Lin, Dissipative generation of significant amount of mechanical entanglement in a coupled optomechanical system, Sci. Rep. **7**, 14497 (2017).

[9] Y.-D. Wang and A. A. Clerk, Reservoir-Engineered Entanglement in Optomechanical Systems, Phys. Rev. Lett. **110**, 253601 (2013).

[10] W. Li, C. Li, and H. Song, Theoretical realization and application of parity-time-symmetric oscillators in a quantum regime, Phys. Rev. A **95**, 023827 (2017).

[11] K. V. Kepesidis, T. J. Milburn, J. Huber, K. G. Makris, S. Rotter, and P. Rabl, PT-symmetry breaking in the steady state of microscopic gain-loss systems, New J. Phys. **18**, 095003 (2016).

[12] C.-G. Liao, R.-X. Chen, H. Xie, M.-Y. He, and X.-M. Lin, Quantum synchronization and correlations of two mechanical resonators in a dissipative optomechanical system, Phys. Rev. A **99**, 033818 (2019).

[13] W. Li, P. Piergentili, J. Li, S. Zippilli, R. Natali, N. Malossi, G. Di Giuseppe, and D. Vitali, Noise robustness of synchronization of two nanomechanical resonators coupled to the same cavity field, Phys. Rev. A **101**, 013802 (2020).

[14] J. Li, R. Yu, and Y. Wu, Proposal for enhanced photon blockade in parity-time-symmetric coupled microcavities, Phys. Rev. A **92**, 053837 (2015).

[15] S. Singh, H. Jing, E. M. Wright, and P. Meystre, Quantum-state transfer between a Bose-Einstein condensate and an optomechanical mirror, Phys. Rev. A **86**, 021801(R) (2012).

[16] D.-X. Li, X.-M. Liao, and X.-Q. Shao, One-way quantum state transfer in a lossy coupled-cavity array, Opt. Express **27**, 35971 (2019).

[17] M. Aspelmeyer, T. J. Kippenberg, and F. Marquardt, Cavity optomechanics, Rev. Mod. Phys. **86**, 1391 (2014).

[18] J. Gieseler, B. Deutsch, R. Quidant, and L. Novotny, Subkelvin Parametric Feedback Cooling of a Laser-Trapped Nanoparticle, Phys. Rev. Lett. **109**, 103603 (2012).

[19] J. Gieseler, L. Novotny, and R. Quidant, Thermal nonlinearities in a nanomechanical oscillator, Nat. Phys. **9**, 806 (2013).

[20] E. Hebestreit, M. Frimmer, R. Reimann, and L. Novotny, Sensing Static Forces with Free-Falling Nanoparticles, Phys. Rev. Lett. **121**, 063602 (2018).

[21] G. Ranjit, M. Cunningham, K. Casey, and A. A. Geraci, Zeptonewton force sensing with nanospheres in an optical lattice, Phys. Rev. A **93**, 053801 (2016).

[22] P. Kumar and M. Bhattacharya, Magnetometry via spin-mechanical coupling in levitated optomechanics, Opt. Express **25**, 19568 (2017).

[23] J. Ahn, Z. Xu, J. Bang, P. Ju, X. Gao, and T. Li, Ultrasensitive torque detection with an optically levitated nanorotor, Nat. Nanotechnol. **15**, 89 (2020).

[24] W. Ge and M. Bhattacharya, Single and two-mode mechanical squeezing of an optically levitated nanodiamond via dressed-state coherence, New J. Phys. **18**, 103002 (2016).

[25] F. Ricci, R. A. Rica, M. Spasenovic, J. Gieseler, L. Rondin, L. Novotny, and R. Quidant, Optically levitated nanoparticle as a model system for stochastic bistable dynamics, Nat. Commun. **8**, 15141 (2017).

[26] O. Romero-Isart, M. L. Juan, R. Quidant, and J. I. Cirac, Toward quantum superposition of living organisms, New J. Phys. **12**, 033015 (2010).

[27] S. Sharma, and M. Bhattacharya, Generating quantum superposition states in a levitated nanodiamond, J. Opt. Soc. Am. B **37**, 1620 (2020).

[28] R. M. Pettit, W. Ge, P. Kumar, D. R. L.-Martin, J. T. Schultz, L. P. Neukirch, M. Bhattacharya, and A. N. Vamivakas, An optical tweezer phonon laser, Nat. Photonics **13**, 402 (2019).

[29] M. Frimmer, J. Gieseler, and L. Novotny, Levitated nanoparticle as a classical two-level atom [Invited], J. Opt. Soc. Am. B **34**, C52 (2017).

[30] H. Jing, S. K. Özdemir, X.-Y. Lü, J. Zhang, L. Yang, and F. Nori, $\mathcal{PT}$-Symmetric Phonon Laser, Phys. Rev. Lett. **113**, 053604 (2014).

[31] J. Naikoo, K. Thapliyal, S. Banerjee, and A. Pathak, Quantum Zeno effect and nonclassicality in a $\mathcal{PT}$-symmetric system of coupled cavities, Phys. Rev. A **99**, 023820 (2019).

[32] J. Peřina, Jr., A. Lukš, J. K. Kalaga, W. Leoński, and A. Miranowicz, Nonclassical light at exceptional points of a quantum $\mathcal{PT}$-symmetric two-mode system, Phys. Rev. A **100**, 053820 (2019).

[33] K. Hammerer, M. Wallquist, C. Genes, M. Ludwig, F. Marquardt, P. Treutlein, P. Zoller, J. Ye, and H. J. Kimble, Strong Coupling of a Mechanical Oscillator and a Single Atom, Phys. Rev. Lett. **103**, 063005 (2009).

[34] A. Roulet and C. Bruder, Quantum Synchronization and Entanglement Generation, Phys. Rev. Lett. **121**, 063601 (2018).

[35] R. Shaniv and R. Ozeri, Quantum lock-in force sensing using optical clock Doppler velocimetry, Nat. Commun. **8**, 14157 (2017).

[36] R. J. Smith, F. Pérez-Cota, L. Marques, and M. Clark, 3D phonon microscopy with sub-micron axial-resolution, Sci. Rep. **11**, 3301 (2021).

[37] S.-L. Zhu, C. Monroe, and L.-M. Duan, Trapped Ion Quantum Computation with Transverse Phonon Modes, Phys. Rev. Lett. **97**, 050505 (2006).

[38] J. Rieser, M. A. Ciampini, H. Rudolph, N. Kiesel, K. Hornberger, B. A. Stickler, M. Aspelmeyer, and U. Delic, Observation of strong and tunable light-induced dipole-dipole interactions between optically levitated nanoparticles, arXiv:2203.04198.

[39] M. Frimmer, J. Gieseler, and L. Novotny, Cooling Mechanical Oscillators by Coherent Control, Phys. Rev. Lett. **117**, 163601 (2016).

[40] B. Rodenburg, L. P. Neukirch, A. N. Vamivakas, and M. Bhattacharya, Quantum model of cooling and force sensing with an optically trapped nanoparticle, Optica **3**, 318 (2016).

[41] G. S. Agarwal and S. Huang, Electromagnetically induced transparency in mechanical effects of light, Phys. Rev. A **81**, 041803(R) (2010).

[42] T. A. Kuusela, Measurement of the second-order coherence of pseudothermal light, Am. J. Phys. **85**, 289 (2017).

[43] R. Loudon, *The Quantum Theory of Light*, 3rd ed. (Oxford University, Oxford, England, 2000).

[44] X.-W. Xu, Y.-x. Liu, C.-P. Sun, and Y. Li, Mechanical $\mathcal{PT}$ symmetry in coupled optomechanical systems, Phys. Rev. A **92**, 013852 (2015).

[45] H. Xu, D.-G. Lai, Y.-B. Qian, B.-P. Hou, A. Miranowicz, and F. Nori, Optomechanical dynamics in the $\mathcal{PT}$- and broken-$\mathcal{PT}$-symmetric regimes, Phys. Rev. A **104**, 053518 (2021).

[46] J. Cuevas, P. G. Kevrekidis, A. Saxena, and A. Khare, $\mathcal{PT}$-symmetric dimer of coupled nonlinear oscillators, Phys. Rev. A **88**, 032108 (2013).

[47] I. V. Barashenkov, D. E. Pelinovsky, and P. Dubard, Dimer with gain and loss: Integrability and $\mathcal{PT}$-symmetry restoration, J. Phys. A: Math. Theor. **48**, 325201 (2015).

[48] S. Vashahri-Ghamsari, B. He, and M. Xiao, Continuous-variable entanglement generation using a hybrid $\mathcal{PT}$-symmetric system, Phys. Rev. A **96**, 033806 (2017).

[49] E. A. Ostrovskaya, Y. S. Kivshar, M. Lisak, B. Hall, F. Cattani, and D. Anderson, Coupled-mode theory for Bose-Einstein condensates, Phys. Rev. A **61**, 031601(R) (2000).

[50] K. Burrage, I. Lenane, and G. Lythe, Numerical methods for second-order stochastic differential equations, SIAM J. Sci. Comput. **29**, 245 (2007).

[51] C. Gardiner, *Stochastic Methods: A Handbook for the Natural and Social Sciences*, 4th ed. (Springer, Berlin, 2010).

[52] I. I. Arkhipov, A. Miranowicz, F. Minganti, and F. Nori, Liouvillian exceptional points of any order in dissipative linear bosonic systems: Coherence functions and switching between $\mathcal{PT}$ and anti-$\mathcal{PT}$ symmetries, Phys. Rev. A **102**, 033715 (2020).

[53] A. Lupu, H. Benisty, and A. Degiron, Switching using $\mathcal{PT}$ symmetry in plasmonic systems: Positive role of the losses, Opt. Express **21**, 21651 (2013).

[54] X. Zhou, and Y. D. Chong, *PT* symmetry breaking and nonlinear optical isolation in coupled microcavities, Opt. Express **24**, 6916 (2016).

[55] K. Stannigel, P. Rabl, A. S. Sørensen, M. D. Lukin, and P. Zoller, Optomechanical transducers for quantum-information processing, Phys. Rev. A **84**, 042341 (2011).

[56] F. Monteiro, W. Li, G. Afek, C.-L. Li, M. Mossman, and D. C. Moore, Force and acceleration sensing with optically levitated nanogram masses at microkelvin temperatures, Phys. Rev. A **101**, 053835 (2020).

[57] Jonas Schäfer, H. Rudolph, K. Hornberger, and B. A. Sticker, Cooling Nanorotors by Elliptic Coherent Scattering, Phys. Rev. Lett. **126**, 163603 (2021).

[58] U. Delic, M. Reisenbauer, D. Grass, N. Kiesel, V. Vuletic, and M. Aspelmeyer, Cavity Cooling of a Levitated Nanosphere by Coherent Scattering, Phys. Rev. Lett. **122**, 123602 (2019).

[59] T. H. Oosterkamp, M. Poggio, C. L. Degen, H. J. Mamin, and D. Rugar, Frequency domain multiplexing of force signals with application to magnetic resonance force microscopy, Appl. Phys. Lett. **96**, 083107 (2010).

[60] F. Y. Khalili and E. Zeuthen, Quantum limits for stationary force sensing, Phys. Rev. A **103**, 043721 (2021).